ACS APPLIED ENERGY MATERIALS

Open Access

This article is licensed under CC-BY 4.0

www.acsaem.org

Letter

Co, Ni-Free Ultrathick Free-Standing Dry Electrodes for Sustainable Lithium-Ion Batteries

Milan K. Sadan, Guo J. Lian, Rachel M. Smith, and Denis Cumming*

Cite This: *ACS Appl. Energy Mater.* 2023, 6, 12166−12171

Read Online

ACCESS | Metrics & More | Article Recommendations | Supporting Information

ABSTRACT: The conventional method of manufacturing lithium-ion battery electrodes employs a complex slurry casting process with solvents that are not environmentally friendly and process parameters that are often difficult to control. This study explores a solvent-free dry electrode fabrication process of Co- and Ni-free $LiMn_2O_4$ (LMO) cathodes using a fibrillated polymer, polytetrafluoroethylene (PTFE). A thick, dry electrode (265−368 μm, 30−64 mg cm^{-2}) of LMO cathode was prepared successfully for the first time. Altering the conductive additives in the LMO dry electrode revealed multiwalled carbon nanotubes (CNTs) as the best conducting agent for dry electrode formulation in terms of conductivity and rate performance. Additionally, an all-dry electrode full cell consisting of both a dry electrode cathode (LMO) and an anode (LTO) delivered a stable cycling performance with a capacity retention of 82.8% after 200 cycles, demonstrating the scope for all-dry electrode full cells for future applications.

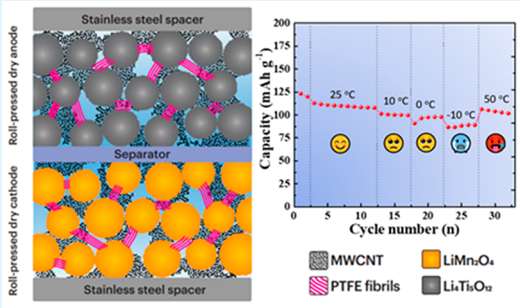

KEYWORDS: *lithium-ion batteries, Co, Ni-free, electric vehicles*

With the increasing prevalence of electric vehicles and the global commitment to achieving net zero carbon emissions by 2050, the development of energy storage devices is anticipated to escalate worldwide.[1,2] Lithium-ion battery (LIB) technology is one of the most promising energy storage technologies due to its lightweight and well-established chemistries.[3] Although LIBs are the ideal candidate that can aid the establishment of renewable green energies via efficient storage, their manufacturing processes are currently energy and resource intensive, typically needing ∼50 kWh of electricity to produce 1 kWh of battery storage.[4−6] Currently, battery electrodes are manufactured by a wet slurry route in which active and additive powders are mixed with toxic organic solvents, such as *N*-methyl-2-pyrrolidone (NMP), which is widely used for cathode manufacture. The NMP solvent is toxic to the environment, and exposure causes severe health hazards to humans.[7] Additionally, the energy needed for electrode drying and solvent recovery forms a large part of the electrode manufacturing cost (∼78%) during the manufacturing of battery electrodes.[8−10] Apart from that, the wet slurry route is susceptible to huge variations in the final microstructure of the electrode due to the uncontrollable binder-carbon migration during the solvent evaporation process[11−13] which results in nonuniform distribution of pores and deteriorates the performance and lifetime of the cell.[14,15] It is imperative that we address all of these issues and find clean manufacturing strategies that can facilitate a sustainable future.

Dry electrode fabrication is an exciting pathway toward sustainable electrode manufacturing that avoids the use of conventional toxic solvents, although the use of polytetrafluoroethylene (PTFE) comes with other challenges. In general, dry electrode fabrication can be classified into three techniques: electrostatic spray dried (ESD) electrodes,[16,17] soft template (holey graphene) assisted electrodes,[18,19] and fibrillation of the binder.[10,20−24] The ESD method involves an additional high-voltage source, and the scalability of the method is debatable.[25,26] The holey graphene-assisted electrode has limitations associated with the additional inactive component and requires high pressure for the electrode roll-to-roll fabrication.[10] The third method is currently the most affordable on a manufacturing scale and requires only slight adjustments in the current manufacturing lines.[15,24] By using a fibrillation polymer (e.g., PTFE), the electrode thickness can be tuned without the binder-carbon migration phenomenon which on its own is the main advantage.[10] Moreover, thick dry electrodes can sufficiently reduce the pack size and increase the overall energy density of the pack, favoring practical applications.[20,27]

In this study, a solvent-free method for creating Co- and Ni-free $LiMn_2O_4$ (LMO) dry electrodes using a fibrillation polymer has been successfully developed for Li-ion batteries. To ensure a sustainable approach, Co- and Ni-free electrodes,

Received: September 28, 2023
Revised: November 29, 2023
Accepted: November 29, 2023
Published: December 8, 2023

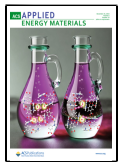

Downloaded via IMPERIAL COLLEGE LONDON on January 31, 2024 at 12:09:59 (UTC).
See https://pubs.acs.org/sharingguidelines for options on how to legitimately share published articles.

ACS Publications

© 2023 The Authors. Published by American Chemical Society

https://doi.org/10.1021/acsaem.3c02448
ACS Appl. Energy Mater. 2023, 6, 12166−12171

LMO, and $Li_4Ti_5O_{12}$ (LTO) were carefully selected as the cathode and anode materials, respectively, in the current study. For this study, we avoided using a graphite negative electrode due to the electrochemical instability of PTFE at low voltage.[15,28,29] Three distinct types of popular, highly conductive carbon were employed to fabricate the dry electrodes, namely, carbon black (CB), carbon nanotube (CNT), and carbon nanofiber (CNF). The electrochemical performance of the LMO dry electrode in both half-cell and full-cell configurations was evaluated with the most optimal conductive agent type. To the best of our knowledge, no reports of dry electrodes based on LMO and LTO half cells, as well as all-dry electrode full cells with LMO/LTO have been published to date. The full cell delivered an excellent capacity retention of 82.8% after 200 cycles.

Figure 1a shows the XRD pattern of the $LiMn_2O_4$ (LMO) particles. The peaks were exactly matching with the spinel $LiMn_2O_4$.[30] Figure 1b and Figure S1 show the SEM images of the LMO particles at different magnifications, revealing their spherical shape and an average diameter of approximately 7 μm. From the EDS mapping shown in Figure 1c, it can be inferred that both manganese and oxygen are equally distributed in the particles.

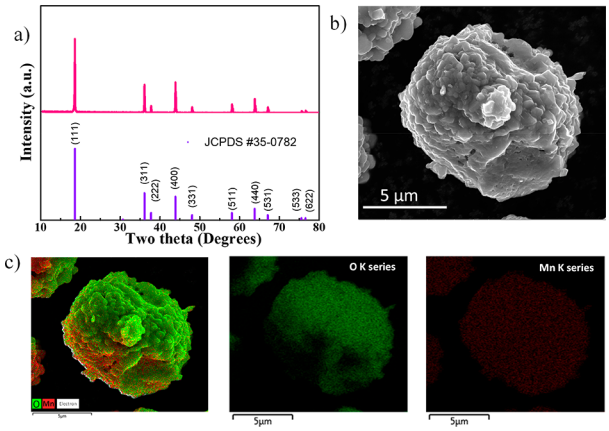

Figure 1. (a) X-ray diffraction (XRD) pattern, (b) scanning electron microscopy (SEM) image, and (c) energy-dispersive X-ray spectroscopy (EDS) mapping of the $LiMn_2O_4$ particles.

LMO dry electrodes with various conductive agents and PTFE were fabricated based on previous reports.[20,31] All the components were mixed in a hot mortar and pestle for several minutes, followed by passing the mixture through a hot roll press at 80 °C to prepare thick, free-standing electrodes (see Supporting Information for details). During the mortar and pestle mixing process, the three-dimensional molecular chains in PTFE transform into a less ordered structure with shear force. The degree of disorder increases further, and the molecular chains slide with each other to form self-assembled fibrils during the hot press calendaring process at 80 °C. Formation of the polymer fibrils yields free-standing dry electrodes.[32] Though the β-transition of PTFE occurs at near room temperature with shear force, Chen et al. reported that the complete fibrillation of PTFE occurs at an elevated temperature >80 °C.[33] Hence, the temperature for hot-roll pressing was selected as 80 °C in the current study. Further, the thickness of dry electrodes was modified by changing the distance between the roll press. Thick electrodes, up to 368 μm, with a high LMO active material loading of 64 mg cm^{-2} were prepared with this process.

The inset of Figure S2 shows the micrograph of the as-prepared freestanding LMO dry electrodes with carbon black (LMO−CB hereafter), carbon nanofiber (LMO−CNF hereafter), and carbon nanotube (LMO−CNT hereafter) as conductive agents. The morphologies of LMO−CB, LMO−CNF, and LMO−CNT are shown in Figure 2a−c, respectively, along with the corresponding EDS mapping images in Figure 2d−f. PTFE fibrils can be seen holding the LMO particles and conductive agents together (indicated by red arrow marks) in all three dry electrodes. The presence of PTFE fibers reinforces the mechanical strength of the electrode structure, generating robust free-standing electrodes.

The electrochemistry of the LMO electrodes (31 mg cm^{-2}) with different carbon conductive agents was analyzed in 6.1 mAh half cells as shown in Figure 3. The rate performance of the electrodes was carried out in constant current and constant voltage mode at different current rates (C-rates), and the corresponding voltage profiles are shown in Figures 3a−d. Although, at low C-rates, the capacities of various LMO electrodes were identical (Figure S2) in nature with the same initial Coulombic efficiencies of 96% each, at high C-rates, the LMO−CNT electrode showed higher rate performances, yielding reversible capacities of 126, 123, 119, 117, 112, 80, and 46 mAh g^{-1} at 0.05, 0.1, 0.2, 0.3, 0.5, 1.5, and 2 C-rates, respectively.

The Nyquist plot in Figure 3e shows the electrochemical impedance (EIS) of the LMO electrode using different conductive agents, and the fitting parameters have been tabulated in Table S1. The charge transfer resistance (R_{ct}) of the LMO electrodes followed a trend of LMO−CNT < LMO−CNF < LMO−CB. The voltage-drop (iR drop) calculated from the galvanostatic intermittent titration technique (GITT) profile (Figure S3) reveals that the trend of voltage drop is in agreement with the EIS results. The iR drop during the electrochemical reaction followed the order of LMO−CNT < LMO−CNF < LMO−CB. To investigate the reason for this observation, the electronic conductivity of the electrodes was analyzed using a standard four-probe technique. The conductivities of the electrodes were found to follow the trend of LMO−CNT > LMO−CNF > LMO−CB which can be correlated to the fact that the highly conductive CNT matrix reduces the iR drop in the electrode and facilitates high-rate performances in LMO dry electrodes. Consequently, the optimized CNT-containing LMO dry electrodes were considered for further analysis.

Cyclic voltammetry of the LMO−CNT electrodes was carried out, as shown in Figure 4a. The characteristic anodic peaks observed at 4.08 V and 4.21 V and cathodic peaks at 4.04 V and 3.91 V, respectively, were consistent with the previous reports on LMO.[30,34] The cycling performance of the LMO−CNT sample at progressively increasing active material loadings up to 29 mg was measured, as shown in Figure 4b. The half cells showed a capacity retention of 93.3, 92.7, and 87.7% at loadings of 10, 16, and 29 mg cm^{-2}, respectively. Notably, the areal capacities are comparable with previous LMO slurry cast reports with similar thickness.[30] Moreover, the cycling performance of the LMO−CNT at a very high loading of 64 mg cm^{-2} was carried out at 0.1 C-rate and is shown in Figure S4 which shows excellent cycling performance up to 50 cycles with a capacity retention of 78%. Additionally, the cycling performance of the LMO−CNT at different

https://doi.org/10.1021/acsaem.3c02448
ACS Appl. Energy Mater. 2023, 6, 12166−12171

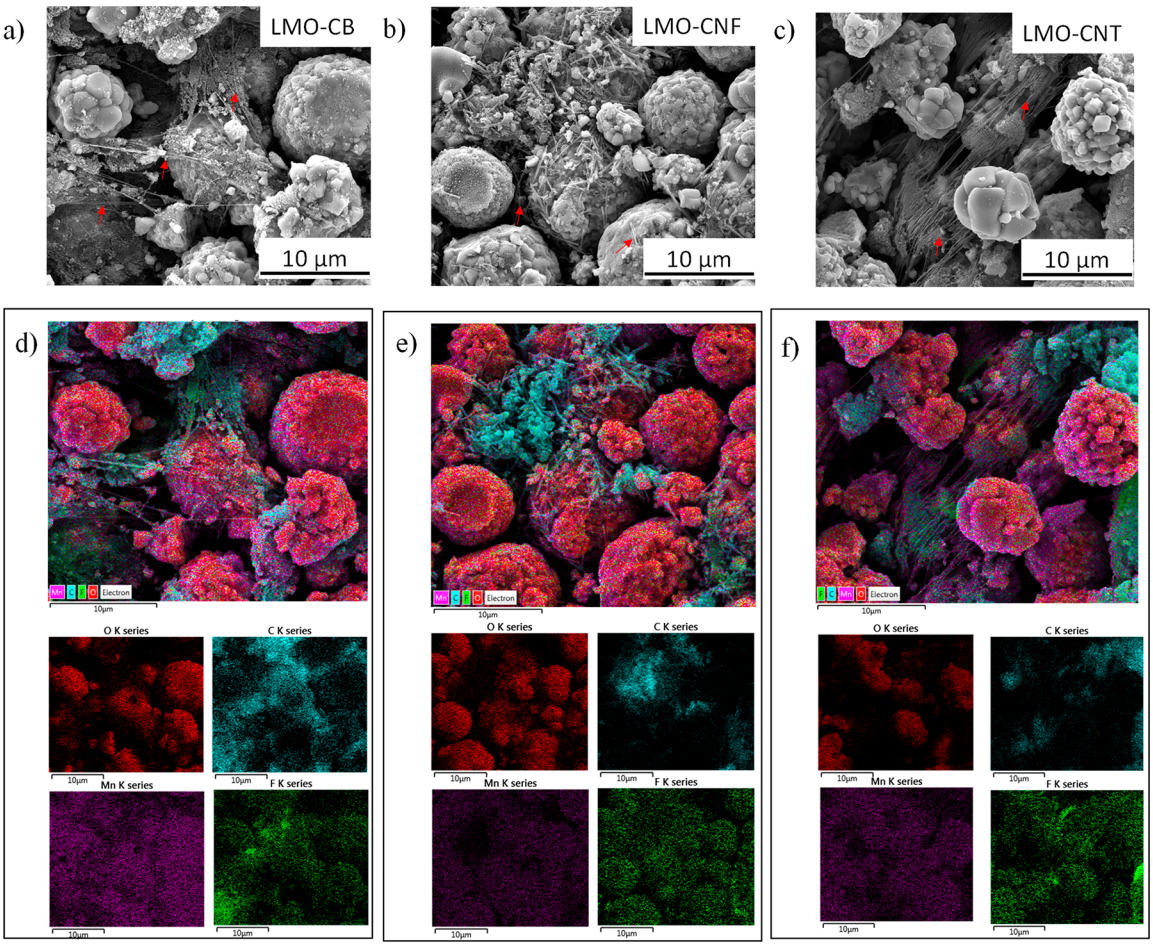

Figure 2. SEM image of LMO electrodes with different conductive agents: (a) carbon black, (b) carbon nanofiber, and (c) carbon nanotube (red arrow indicates the polymer fibrils). EDS mapping of LMO electrode with different conductive agents: (d) carbon black, (e) carbon nanofiber, and (f) carbon nanotube.

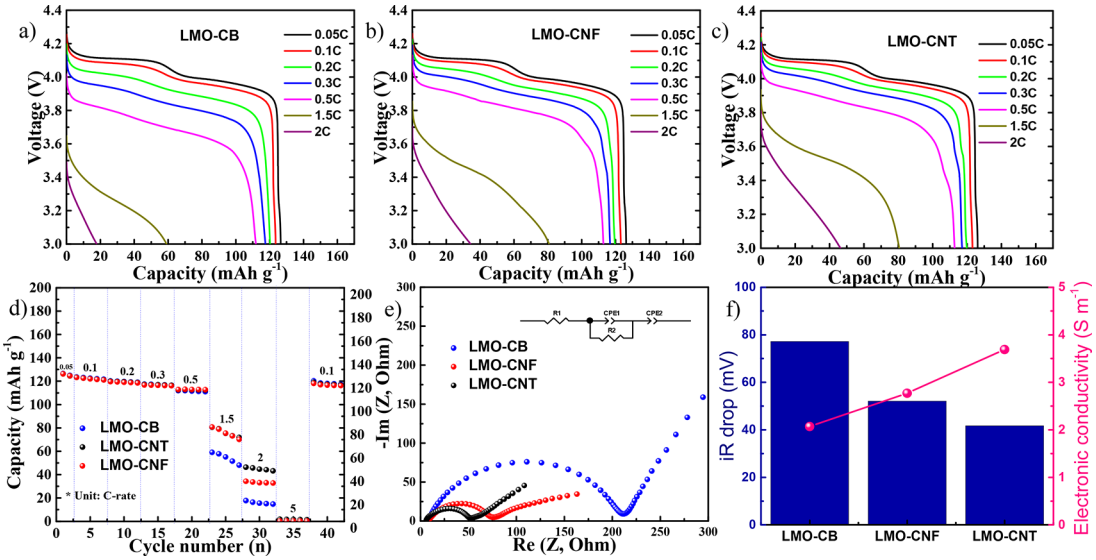

Figure 3. Discharge curves of 30 mg cm^{-2} LMO electrodes with (a) CB, (b) CNF, and (c) CNT conductive agents at different current densities (1C = 148 mAh g^{-1}). Comparison of (d) rate performances, (e) Nyquist plot, and (f) voltage drop/electronic conductivity of the LMO cathode with different conductive agents.

ambient temperatures (Figure 4c) was evaluated at a 0.2 C-rate. The LMO−CNT showed a capacity of 123, 114, 108, 99, and 129 mAh g^{-1} at different temperatures of 25, 10, 0, −10, and 50 °C, respectively. The capacities were less affected by the ambient temperature, which could be due to the excellent electronic conductivity of the LMO−CNT electrode.

https://doi.org/10.1021/acsaem.3c02448
ACS Appl. Energy Mater. 2023, 6, 12166−12171

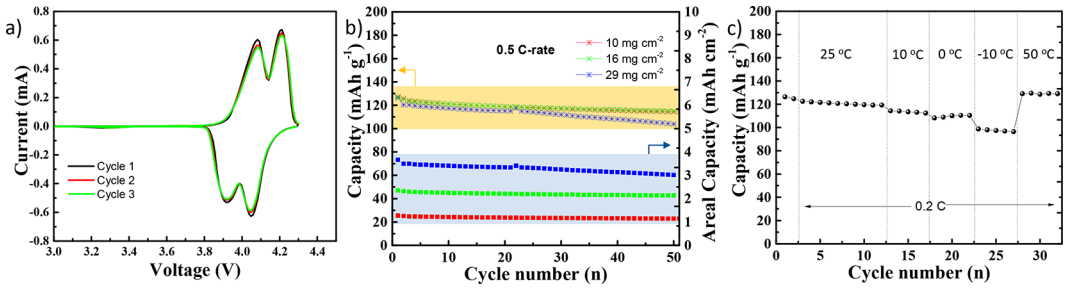

Figure 4. (a) Cyclic voltammetry (CV) at a scan rate of 0.1 mV s^{-1}, (b) cycling performance at 0.5 C-rate of the LMO−CNT electrode at different loading, and (c) cycling performance of the LMO−CNT electrode at 0.2 Crate at various ambient temperatures.

In order to make freestanding all-dry electrode full cells, commercial lithium titanate ($Li_4Ti_5O_{12}$, LTO) was selected as the anode material. The XRD, SEM, and EDS mapping of the LTO particles showed pure phase material with a particle size of about 900 nm. The electrochemical performance of the LTO−CNT dry electrode is shown in Figure S6. The cyclic voltammetry of the LTO−CNT (Figure S6a) shows single oxidation and reduction peaks at 1.78 V and 1.35 V, respectively. The voltage profile at 0.05 C-rate (Figure S6b) exhibited a single plateau that supports the CV results. Further, the cycling performance of the LTO anode at 0.5C in Figure S6c shows an excellent reversible capacity of 170 mAh g^{-1} with 60% capacity retention after 50 cycles. The rate performance of the LTO−CNT electrode is shown in Figure S6d with a reversible capacity of 122.1, 80.3, 43.6, 20.2, and 4.3 mAh g^{-1} at 0.1, 0.2, 0.5, 1, and 2C, respectively. Figure S6e shows the EIS spectrum of the LTO−CNT electrode with a charge transfer resistance of ∼200 Ω which is slightly higher than the previously reported LTO thick electrodes prepared via a wet route and can be attributed to the comparatively thicker LTO electrodes (360 μm) utilized in the current study as opposed to previous reports.[35,36] Further, it should be noted that the GITT profile (Figure S6f) of the LTO−CNT shows a low *iR* drop of 0.02 V at a 0.1 C-rate.

All dry electrode full cells with LMO−CNT and LTO−CNT were assembled, and the electrochemical performances are shown in Figure 5. Figure 5a shows the CV of the LMO−CNT/LTO−CNT full cell at a scan rate of 0.2 mV s^{-1}. Two oxidation peaks and reduction peaks were merged at around 2.4 V and 2.1 V, respectively. The rate performance and corresponding voltage profile at different C-rates are shown in Figures 5b and S7a, respectively. The full cell showed a capacity of 110.4, 99.0, 82.7, 71.6, 52.1, and 6.8 mAh g^{-1} at a C-rate of 0.05, 0.1, 0.2, 0.3, 0.5, and 1C, respectively. When the current density was reduced to a 0.1 C-rate, a capacity of 91.2 was obtained, which shows high stability for full cells. The full cells were cycled at a 0.7 C-rate and a stable cycle performance with a capacity retention of 82.8% after 200 cycles. The Nyquist plot shown in Figure S7b shows a low charge transfer resistance of ∼100 Ω. In addition, the full cell exhibited excellent capacities at various ambient temperatures from −10 to 50 °C (Figure 5d), indicating promising prospects for practical applications

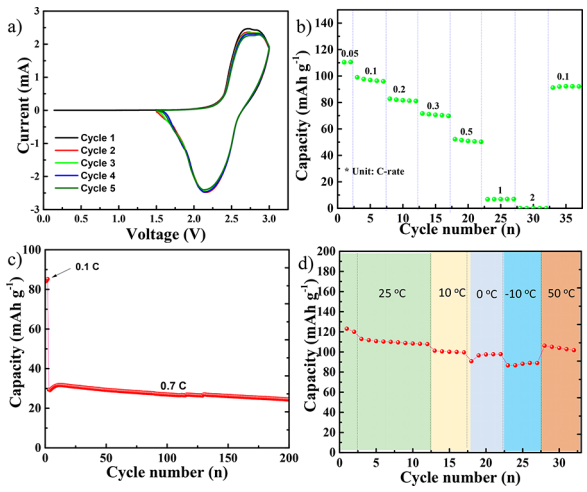

Figure 5. (a) Cyclic voltammetry at a scan rate of 0.2 mV s^{-1}, (b) rate performance, (c) cycling performance, and (d) cycling performance at different ambient temperatures at a current rate of 0.2C of the LMO/LTO all dry full cell.

In summary, Co- and Ni-free all-dry electrode full cells with LMO as the cathode and LTO as the anode were fabricated for the first time. By incorporating CNT as a conductive agent, excellent electronic conductivity and rate performance were achieved from the LMO cathode at varied loading from 10 mg cm^{-2} to 64 mg cm^{-2}. The CNT improved the electrode electronic conductivity and thereby reduced the internal resistance of the electrode, which resulted in the excellent rate performance of the LMO−CNT electrodes compared to LMO−CB and LMO−CNF. With the LMO−CNT cathode and LTO−CNT anode, an all-dry electrode full cell was assembled which delivered a capacity of 110 mAh g^{-1} at 0.05 C-rate. To best of our knowledge, there are no full cell reports based on Ni- and Co-free cathodes in dry electrode fabrication techniques in the field of lithium-ion batteries. The full cells with a high loading exhibited exceptional electrochemical performance at varying temperatures as well, including room temperature, subzero temperature, and elevated ambient temperatures. The sustainable solution demonstrated in this report calls for the commercialization of all-dry electrode cells with a thick $LiMn_2O_4$ cathode material as a viable substitute for the popular cathodes that contain critical elements such as Ni or Co. To understand the specific impact of various conducting agents in the dry processing technique, it is imperative to draw correlations between the porosity and the mechanical properties of the LMO dry electrodes. Additionally, in-depth analysis of the diffusion kinetics and structural evolution of the dry electrodes during electrode processing are critical areas of interest and will be the main scope of our next article.

https://doi.org/10.1021/acsaem.3c02448
ACS Appl. Energy Mater. 2023, 6, 12166−12171

■ ASSOCIATED CONTENT

Supporting Information

The Supporting Information is available free of charge at https://pubs.acs.org/doi/10.1021/acsaem.3c02448.

Experimental details, materials, and electrochemical characterization of LTO dry electrodes (PDF)

■ AUTHOR INFORMATION

Corresponding Author

Denis Cumming − *Department of Chemical and Biological Engineering, University of Sheffield, Sheffield S1 3JD, U.K.; Faraday Institution, Didcot OX11 0RA, U.K.;* orcid.org/0000-0003-1923-2250; Email: d.cumming@sheffield.ac.uk

Authors

Milan K. Sadan − *Department of Chemical and Biological Engineering, University of Sheffield, Sheffield S1 3JD, U.K.; Faraday Institution, Didcot OX11 0RA, U.K.;* orcid.org/0000-0002-4704-5789

Guo J. Lian − *Department of Chemical and Biological Engineering, University of Sheffield, Sheffield S1 3JD, U.K.*

Rachel M. Smith − *Department of Chemical and Biological Engineering, University of Sheffield, Sheffield S1 3JD, U.K.; Faraday Institution, Didcot OX11 0RA, U.K.*

Complete contact information is available at: https://pubs.acs.org/10.1021/acsaem.3c02448

Notes

The authors declare no competing financial interest.

■ ACKNOWLEDGMENTS

The authors thank the financial support provided by the project of "Nextrode" funded by Faraday Institution, UK (Grant number: FIRG015).

■ REFERENCES

(1) Akimoto, K. Assessment of road transportation measures for global net-zero emissions considering comprehensive energy systems. *IATSS Res.* **2023**, *47* (2), 196−203.

(2) Scheller, C.; Kishita, Y.; Blömeke, S.; Thies, C.; Schmidt, K.; Mennenga, M.; Herrmann, C.; Spengler, T. S. Designing robust transformation toward a sustainable circular battery production. *Procedia CIRP.* **2023**, *116*, 408−413.

(3) Mohammadi, F.; Saif, M. A comprehensive overview of electric vehicle batteries market. *e-Prime-Adv. Electr. Eng. Electr. Energy.* **2023**, *3*, 100127.

(4) Liu, J.; Ludwig, B.; Liu, Y.; Zheng, Z.; Wang, F.; Tang, M.; Wang, J.; Wang, J.; Pan, H.; Wang, Y. Scalable Dry Printing Manufacturing to Enable Long-Life and High Energy Lithium-Ion Batteries. *Adv. Mater. Technol.* **2017**, *2* (10), 1700106.

(5) Jinasena, A.; Burheim, O. S.; Strømman, A. H. A Flexible Model for Benchmarking the Energy Usage of Automotive Lithium-Ion Battery Cell Manufacturing. *Batteries* **2021**, *7* (1), 14.

(6) Davidsson Kurland, S. Energy use for GWh-scale lithium-ion battery production. *Environ. Res. Commun.* **2020**, *2* (1), 012001.

(7) Al-Shroofy, M.; Zhang, Q.; Xu, J.; Chen, T.; Kaur, A. P.; Cheng, Y.-T. Solvent-free dry powder coating process for low-cost manufacturing of LiNi1/3Mn1/3Co1/3O2 cathodes in lithium-ion batteries. *J. Power Sources* **2017**, *352*, 187−193.

(8) Wood, D. L.; Li, J.; Daniel, C. Prospects for reducing the processing cost of lithium ion batteries. *J. Power Sources* **2015**, *275*, 234−242.

(9) Turcheniuk, K.; Bondarev, D.; Amatucci, G. G.; Yushin, G. Battery materials for low-cost electric transportation. *Mater. Today* **2021**, *42*, 57−72.

(10) Ryu, M.; Hong, Y. K.; Lee, S. Y.; Park, J. H. Ultrahigh loading dry-process for solvent-free lithium-ion battery electrode fabrication. *Nat. Commun.* **2023**, *14* (1), 1316.

(11) Font, F.; Protas, B.; Richardson, G.; Foster, J. M. Binder migration during drying of lithium-ion battery electrodes: Modelling and comparison to experiment. *J. Power Sources* **2018**, *393*, 177−185.

(12) Müller, M.; Pfaffmann, L.; Jaiser, S.; Baunach, M.; Trouillet, V.; Scheiba, F.; Scharfer, P.; Schabel, W.; Bauer, W. Investigation of binder distribution in graphite anodes for lithium-ion batteries. *J. Power Sources* **2017**, *340*, 1−5.

(13) Klemens, J.; Schneider, L.; Herbst, E. C.; Bohn, N.; Müller, M.; Bauer, W.; Scharfer, P.; Schabel, W. Drying of NCM Cathode Electrodes with Porous, Nanostructured Particles Versus Compact Solid Particles: Comparative Study of Binder Migration as a Function of Drying Conditions. *Energy Technol.* **2022**, *10* (4), 2100985.

(14) Lombardo, T.; Ngandjong, A. C.; Belhcen, A.; Franco, A. A. Carbon-Binder Migration: A Three-Dimensional Drying Model for Lithium-ion Battery Electrodes. *Energy Storage Mater.* **2021**, *43*, 337−347.

(15) Lu, Y.; Zhao, C.-Z.; Yuan, H.; Hu, J.-K.; Huang, J.-Q.; Zhang, Q. Dry electrode technology, the rising star in solid-state battery industrialization. *Matter* **2022**, *5* (3), 876−898.

(16) Schälicke, G.; Landwehr, I.; Dinter, A.; Pettinger, K.-H.; Haselrieder, W.; Kwade, A. Solvent-Free Manufacturing of Electrodes for Lithium-Ion Batteries via Electrostatic Coating. *Energy Technol.* **2020**, *8* (2), 1900309.

(17) Liu, J.; Ludwig, B.; Liu, Y.; Pan, H.; Wang, Y. Strengthening the Electrodes for Li-Ion Batteries with a Porous Adhesive Interlayer through Dry-Spraying Manufacturing. *ACS Appl. Mater. Interfaces* **2019**, *11* (28), 25081−25089.

(18) Zuluaga-Gomez, C. C.; Plaza-Rivera, C. O.; Tripathi, B.; Katiyar, R. K.; Pradhan, D. K.; Morell, G.; Lin, Y.; Correa, M.; Katiyar, R. S. Holey Graphene/Ferroelectric/Sulfur Composite Cathodes for High-Capacity Lithium-Sulfur Batteries. *ACS Omega* **2023**, *8* (14), 13097−13108.

(19) Kirsch, D. J.; Lacey, S. D.; Kuang, Y.; Pastel, G.; Xie, H.; Connell, J. W.; Lin, Y.; Hu, L. Scalable Dry Processing of Binder-Free Lithium-Ion Battery Electrodes Enabled by Holey Graphene. *ACS Appl. Energy Mater.* **2019**, *2* (5), 2990−2997.

(20) Fiedler, M.; Cangaz, S.; Hippauf, F.; Dörfler, S.; Abendroth, T.; Althues, H.; Kaskel, S. Mechanistic Insights into the Cycling Behavior of Sulfur Dry-Film Cathodes. *Adv. Sustain. Syst.* **2023**, DOI: 10.1002/adsu.202200439.

(21) Hu, J.-K.; Yuan, H.; Yang, S.-J.; Lu, Y.; Sun, S.; Liu, J.; Liao, Y.-L.; Li, S.; Zhao, C.-Z.; Huang, J.-Q. Dry electrode technology for scalable and flexible high-energy sulfur cathodes in all-solid-state lithium-sulfur batteries. *J. Energy Chem.* **2022**, *71*, 612−618.

(22) Schmidt, F.; Kirchhoff, S.; Jagle, K.; De, A.; Ehrling, S.; Hartel, P.; Dorfler, S.; Abendroth, T.; Schumm, B.; Althues, H.; Kaskel, S. Sustainable Protein-Based Binder for Lithium-Sulfur Cathodes Processed by a Solvent-Free Dry-Coating Method. *ChemSusChem* **2022**, *15* (22), No. e202201320.

(23) Yao, W.; Chouchane, M.; Li, W.; Bai, S.; Liu, Z.; Li, L.; Chen, A. X.; Sayahpour, B.; Shimizu, R.; Raghavendran, G.; Schroeder, M. A.; Chen, Y.-T.; Tan, D. H. S.; Sreenarayanan, B.; Waters, C. K.; Sichler, A.; Gould, B.; Kountz, D. J.; Lipomi, D. J.; Zhang, M.; Meng, Y. S. A 5 V-class cobalt-free battery cathode with high loading enabled by dry coating. *Energy Environ. Sci.* **2023**, *16* (4), 1620−1630.

(24) Zhang, Y.; Lu, S.; Lou, F.; Yu, Z. Solvent-free lithium iron phosphate cathode fabrication with fibrillation of polytetrafluoroethylene. *Electrochim. Acta* **2023**, *456*, 142469.

(25) Hawley, W. B.; Li, J. Electrode manufacturing for lithium-ion batteries—Analysis of current and next generation processing. *J. Energy Storage* **2019**, *25*, 100862.

(26) Ludwig, B.; Zheng, Z.; Shou, W.; Wang, Y.; Pan, H. Solvent-Free Manufacturing of Electrodes for Lithium-ion Batteries. *Sci. Rep* **2016**, *6*, 23150.
(27) Singh, M.; Kaiser, J.; Hahn, H. Thick Electrodes for High Energy Lithium Ion Batteries. *J. Electrochem. Soc.* **2015**, *162* (7), A1196−A1201.
(28) Shang, Y.; Chu, T.; Shi, B.; Fu, K. Scalable Synthesis of LiF-rich 3D Architected Li Metal Anode via Direct Lithium-Fluoropolymer Pyrolysis to Enable Fast Li Cycling. *Energy Environ.* **2021**, *4* (2), 213−221.
(29) Periyapperuma, K.; Tran, T. T.; Trussler, S.; Ioboni, D.; Obrovac, M. N. Conflat Two and Three Electrode Electrochemical Cells. *J. Electrochem. Soc.* **2014**, *161* (14), A2182−A2187.
(30) Guo, Y.; Li, X.; Wang, Z.; Wang, J.; Guo, H.; Yan, G. Free-standing ultrathick LiMn2O4@single-wall carbon nanotubes electrode with high areal capacity. *J. Energy Chem.* **2022**, *73*, 452−459.
(31) Kim, H. M.; Yoo, B. I.; Yi, J. W.; Choi, M. J.; Yoo, J. K. Solvent-Free Fabrication of Thick Electrodes in Thermoplastic Binders for High Energy Density Lithium-Ion Batteries. *Nanomater.* **2022**, *12* (19), 3320.
(32) Dimitrios, A. V. *Role of fibrillation on Poisson's ratio of expanded polytetrafluoroethylene (PTFE)*; University of British Columbia: Vancouver, 2017.
(33) Lee, D. J.; Jang, J.; Lee, J. P.; Wu, J.; Chen, Y. T.; Holoubek, J.; Yu, K.; Ham, S. Y.; Jeon, Y.; Kim, T. H.; Lee, J. B.; Song, M. S.; Meng, Y. S.; Chen, Z. Physio-Electrochemically Durable Dry-Processed Solid-State Electrolyte Films for All-Solid-State Batteries. *Adv. Funct. Mater.* **2023**, *33* (28), 2301341.
(34) Iskandar Radzi, Z.; Helmy Arifin, K.; Zieauddin Kufian, M.; Balakrishnan, V.; Rohani Sheikh Raihan, S.; Abd Rahim, N.; Subramaniam, R. Review of spinel LiMn2O4 cathode materials under high cut-off voltage in lithium-ion batteries: Challenges and strategies. *J. Electroanal. Chem.* **2022**, *920*, 116623.
(35) Deng, W.; Shi, W.; Liu, Q.; Jiang, J.; Li, X.; Feng, X. Constructing Gradient Porous Structure in Thick Li4Ti5O12 Electrode for High-Energy and Stable Lithium-Ion Batteries. *ACS Sustain. Chem. Eng.* **2020**, *8* (46), 17062−17068.
(36) Cai, C.; Yost, D.; Koenig, G. M. Increased cycling rates for thick all active material electrodes via electrolyte modifications. *J. Energy Storage* **2023**, *64*, 107238.

https://doi.org/10.1021/acsaem.3c02448
ACS Appl. Energy Mater. 2023, 6, 12166−12171